JOURNAL OF GEOPHYSICAL RESEARCH, VOL. 100, NO. A2, PAGES 1795–1809, FEBRUARY 1, 1995

An interpretation of a mysterious 3.0- to 4.6-kHz emission band observed on Voyager 2 near Neptune

Vikas S. Sonwalkar, Umran S. Inan, and Timothy F. Bell

Space, Telecommunications, and Radioscience Laboratory, Stanford University, Stanford, California

Abstract. A whistler mode interpretation is provided for the narrowband signal ($f \sim 3 - 4.6$ kHz, $\Delta f \sim 200 - 800$ Hz) detected by the plasma wave instrument on Voyager 2 during its encounter with Neptune. Our analysis indicates that this signal may have been generated in a limited spatial region and that it propagated to other regions of the Neptunian magnetosphere in the nonducted whistler mode with wave normal vectors lying close to the whistler mode resonance cone. The observed frequency variation of the emission along the Voyager 2 trajectory is consistent with this interpretation. The source location is estimated to be near the magnetic equator at $L \sim 4$ and dipole longitude of 111°W (260°W longitude in Neptune coordinate system). The source frequency and bandwidth are estimated to be 3.6 kHz and 300 Hz, respectively. The waves most likely would have been generated by energetic electrons with 2- to 20-keV parallel energy via a gyroresonance mechanism. Our interpretation of the narrowband emissions places the following limits on the Neptunian thermal plasma density and temperature: (1) $N_{e,\min} > 0.16$ el/cm^3 for $1.2\,R_N < R < 5R_N$, (2) $N_{e,\max}$=597.5 cm^{-3} at $R = 1.3R_N$, (3) $T_{e,\max} < 500-1000°$ K at $R \sim 5R_N$. It is also possible that the weak UV aurora observed near Neptune could have been caused by the precipitation of energetic particles by the narrowband emission as a result of wave particle interactions.

Introduction

The Voyager 2 plasma wave (PWS) instrument detected a narrowband emission (NBE) ($f \sim 3 - 4.6$ kHz, $\Delta f \sim 200 - 800$ Hz) during its close encounter with Neptune [*Gurnett et al.*, 1989; *Moses and Coroniti*, 1991]. Based on the values of the local plasma parameters, electron density N_e and magnetic field $\mathbf{B}_0$, the signal is expected to propagate in the whistler mode [*Gurnett et al.*, 1989]. In general, the frequencies of naturally occurring whistler mode signals observed in the terrestrial magnetosphere show a close association with local (or equatorial) gyrofrequency. The narrowband signal observed in the Neptunian magnetosphere is somewhat mysterious because its frequency varied very little over a wide range of local gyrofrequency f_{he} (280 - 4.7 kHz) along the Voyager 2 orbit. *Moses and Coroniti* [1991] suggested that the emission may be Z mode radiation similar to the trapped Z mode waves (with frequencies close to the left-hand cutoff frequency) found in the terrestrial and Jovian magnetospheres.

In this paper we provide a new whistler mode interpretation of the narrowband signal. We show that it is possible that the NBE was generated in a limited spatial region and that it propagated to other regions of the Neptunian magnetosphere in the nonducted whistler mode with wave normal vectors lying close to the whistler mode resonance cone. This interpretation is consistent with the observed frequency variation of the emission along the Voyager 2 orbit and allows us to place certain limits on the Neptunian plasma density and temperature.

Observations

Figure 1a shows an example of the narrowband emission that is the subject of this paper. Of the 78 wideband data frames (each ~48 s or less long) collected by PWS near Neptune during 2036 spacecraft event time (SCET) (day 236) to 1230 SCET (day 237) (see *Scarf and Gurnett* [1977] for the details of PWS), the NBE appeared in 29 wideband frames, all during 0310 - 0538 SCET on day 237. Figure 1b shows a mosaic of all the wideband frames containing the NBE. (See Plates 1 and 2 of *Moses and Coroniti* [1991] for a colored version of Figure 1.) Figure 2 shows the upper and lower frequency cutoff of the emission (as scaled from spectra similar to one shown in Figure 1a) observed along the Voyager 2 orbit. The actual bandwidth of the signal is probably higher than that shown in this figure because the wideband receivers with automatic gain control (AGC) tend to suppress weak signals [*Sonwalkar and Inan*, 1989]. Though wideband data frames were also obtained between 0330 SCET and 0400 SCET and between 0440 and 0515 SCET, no emissions of any kind were observed during these periods because the AGC was set by strong dust impact signals during the ring plane crossings [*Moses and Coroniti*, 1991]. Wideband data frames available before 0310 (the first such frame was available at 0255 SCET) and after 0538 SCET (the first such frame was available at 0602 SCET) also showed no sign of NBE.

Figures 3a ,3b, 3c, and 3d show the radial distance, latitude, west-longitude, and local time, respectively, of the Voyager 2 orbit during the period when NBE was observed. For our purpose it is more appropriate to represent the trajectory of Voyager 2 near Neptune in a magnetic coordinate frame that rotates with the planet. We use an offset tilted dipole (OTD2) coordinate frame identical to that employed by *Cheng* [1990]. In this frame the origin is at the center of the dipole which is $0.55R_N$ from the center of the planet. The z axis is along the dipole axis which is tilted 45.2° from the rotation axis and toward −76.5° longitude. The x axis is defined such that the vector joining the dipole center to the planet center falls in the $z - x$ plane and the y axis is defined by the right-hand rule. Thus in this frame the dipole latitude and longitude of a vector are given by $\lambda_m = 90 - \theta_m$ and ϕ_m, where θ_m and ϕ_m are the polar and the azimuthal angles, respectively. Figures 4a, b, and c show the Voyager 2 orbit parameters (the distance from the dipole center R_m, dipole latitude λ_m, and longitude ϕ_m) in this coordinate

Paper number 94JA02678.
0148-0227/95/94JA-02678$05.00

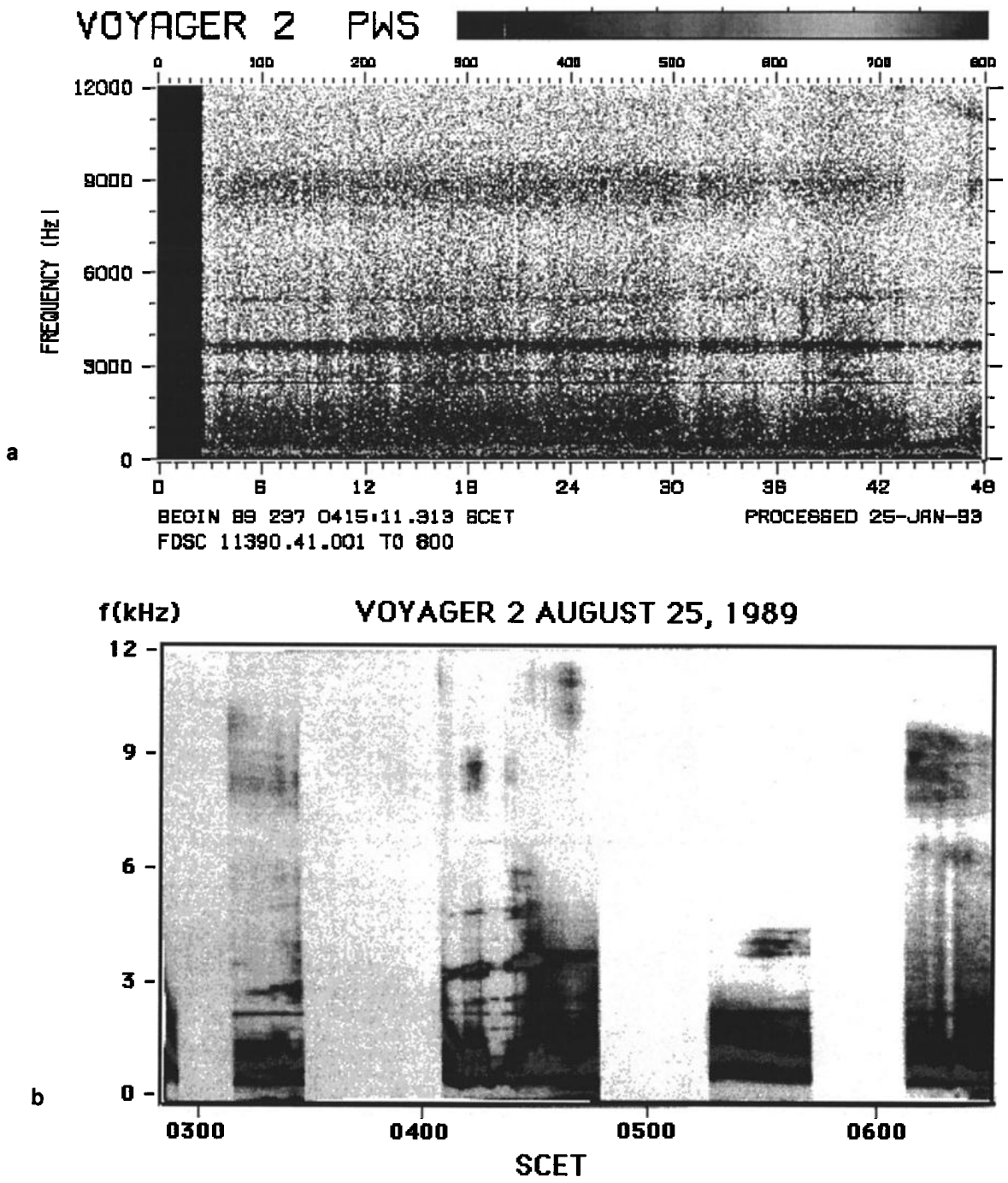

Figure 1. (a) Typical wideband frame from closest approach. This figure presents a 48-s wideband frame from 0415:11 SCET. The narrowband emission (NBE) near 3.3 kHz is the subject of this paper. (b) Mosaic of the 29 wideband frames from the closest approach that showed NBE. The NBE frequency is observed to increase from 3 kHz at 0300 SCET to 4.6 kHz at 0540 SCET [From *Moses and Coroniti*, 1991].

system during the period when NBE was observed. Figures 5 and 6 show the projection of the Voyager 2 trajectory onto the dipole meridional and equatorial planes, respectively.

The salient features of the NBE observed near Neptune are: (1) the emission was observed between 0310-0538 SCET over wide ranges of radial distances (1.2 - $5R_N$), dipole latitudes (λ_m = 20° S – 70° N), and longitudes (180° W – 50° E), (2) the strongest signals were observed between 0405 and 0432 SCET, (3) except for a relatively weak signal at 3.7 kHz that was observed at 0310 SCET, the average emission frequency generally increased monotonically with time from ~ 3 kHz at 0319 SCET to 4.6 kHz at 0538 SCET, (4) the emission bandwidth varied between ~ 200 Hz and ~ 800 Hz, with the largest bandwidth observed near 0538 SCET, and (5) the local time of the observations was ~ 1300 before 0340 SCET and 0100 after 0400 SCET. The local gyrofrequency during the period when NBE was observed varied between ~ 4.7 kHz and 280 kHz with smaller values of gyrofrequency observed at later times.

Interpretation

The analysis approach used in this work is based on a formalism developed by *Sonwalkar* [1986] to analyze satellite plasma

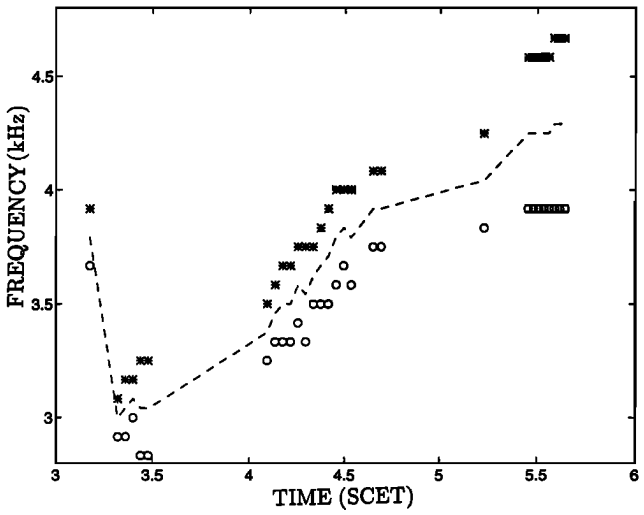

Figure 2. The upper and lower frequency cutoff of the NBE observed along the Voyager 2 orbit. The dashed line shows the average frequency of the signal.

wave data. In this formalism the kinetic constraints arising from the physics of the medium (i.e., properties such as cutoffs, dispersion, polarization of the modes of propagation) and the kinematic constraints arising from the measurement process (i.e., motion of the satellite, response of the detector, receiver characteristics, sampling rate of the data) are explicitly taken into account to predict certain quantities that can be tested experimentally. The method is particularly useful in situations such as that of the Voyager 2 data from Neptune, in which more direct tests of a given hypothesis are not possible due to experimental limitations.

The Hypotheses

We put forth the following hypotheses concerning the nature of the NBE and test them by application of the *Sonwalkar* [1986] formalism:

1. The narrowband signal was generated in a region confined to longitudes where the strongest signals were observed. Nominally, we assume that the NBE was generated with $f \sim 3.58$ kHz and within a bandwidth of $\Delta f \sim 200 - 300$ Hz near the 250° dipole longitude meridional plane. These values correspond to the average frequency and bandwidth of the signal and the dipole longitude of Voyager 2 at 0415 SCET when the strongest NBE was observed (to the degree that as determined from the AGC controlled response of the wideband receiver). We show below that our results are not very sensitive to the exact location and the frequency of the source.
2. The signals propagated from the source region to the observation points in the nonducted whistler mode, with wave normal vectors lying close to the whistler mode resonance cone.
3. The observed frequency and bandwidth variations of the emission result from the Doppler shifts introduced by the motion of the spacecraft.

Figure 7 schematically shows the propagation of NBE from the assumed source location to various observations points along the Voyager 2 trajectory. Hypothesis 1 is consistent with the observation that the signal frequency remained nearly constant even though the local gyrofrequency varied widely. It is also consistent with the observation that weaker signals were observed before and after Voyager 2 crossed the presumed source location.

Hypothesis 2 is consistent with the known propagation characteristics of nonducted whistler mode signals in the terrestrial magnetosphere. In general, whistler mode waves at a given frequency f generated within the magnetosphere (or from a source below the

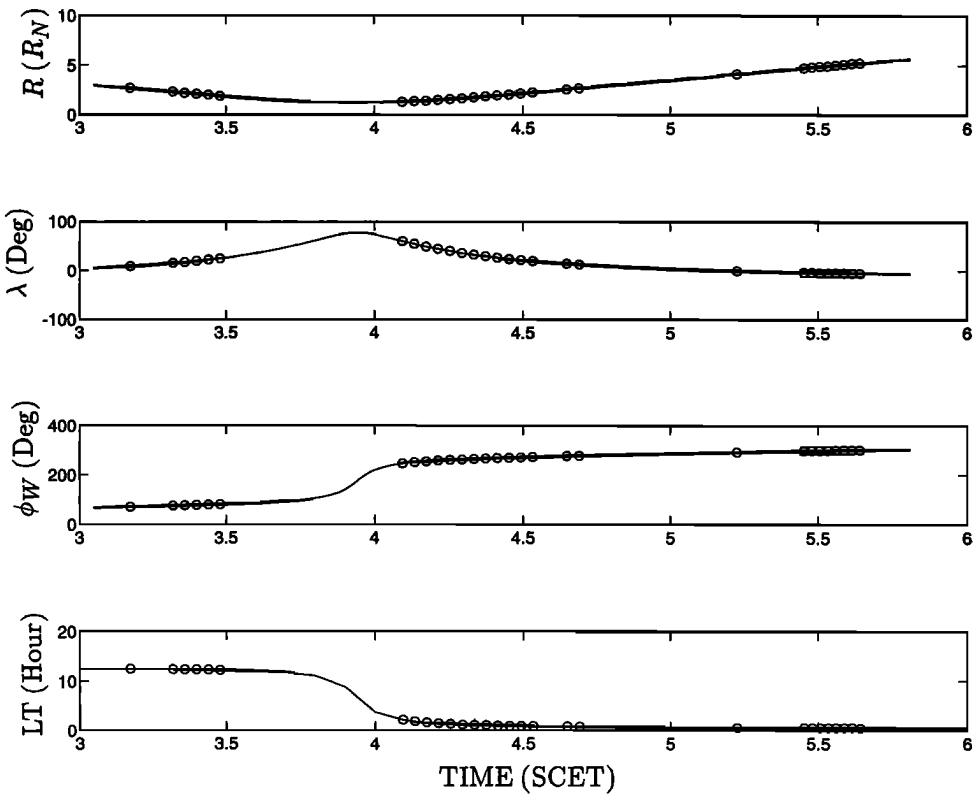

Figure 3. The radial distance R, latitude λ, west-longitude ϕ_W, and local time (LT) of the Voyager 2 orbit in Neptune coordinate system when the NBE was observed. The circles indicate locations of Voyager 2 at times when the 29 wideband frames showing the NBE were obtained.

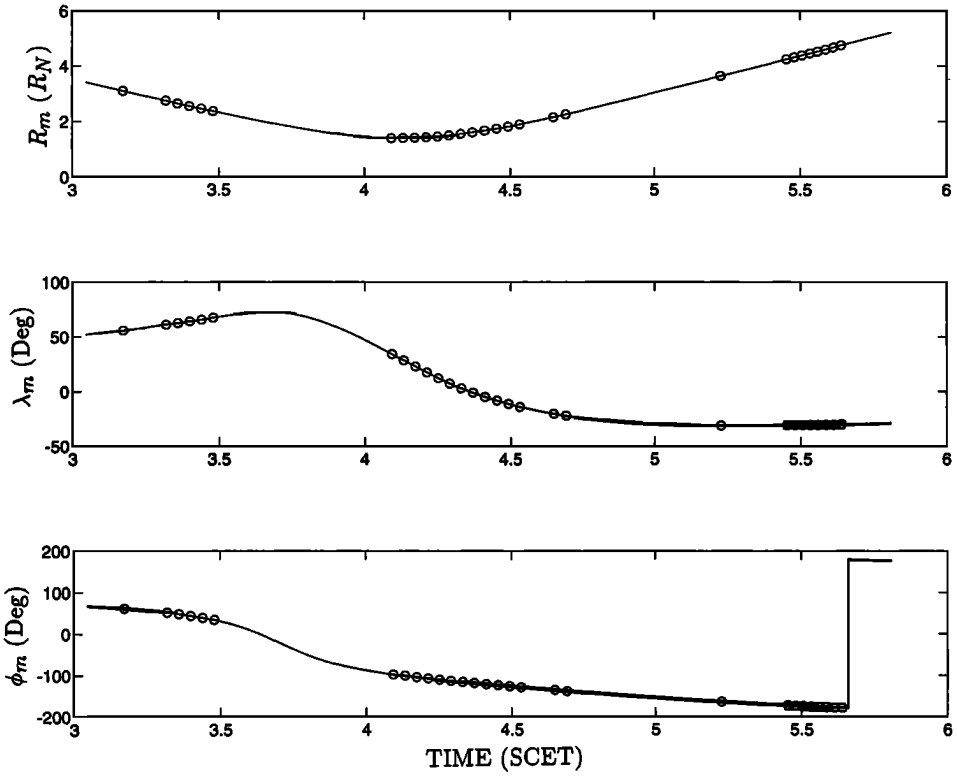

Figure 4. The Voyager 2 orbit parameters in OTD2 coordinate system when NBE was observed: the distance from the dipole center R_m, dipole latitude λ_m and longitude ϕ_m. The circles indicate locations of Voyager 2 at times when the 29 wideband frames showing the NBE were obtained.

ionosphere) remain trapped within the magnetosphere, bouncing back and forth between the two hemispheres (see Figure 7) [*Kimura*, 1966, *Edgar*, 1976]. In each hemisphere the waves are reflected at points where $f = f_{LHR}$, where f_{LHR} is the local lower hybrid resonance frequency. After the first magnetospheric reflection the wave normal vectors are generally close (within a few degrees) to the resonance cone and remain so during the subsequent bounces [*Edgar*, 1976]. If such waves were generated with a nonzero component of the wave vector in the azimuthal direction, and if the Landau damping of the waves were insignificant, they can drift considerably in longitude, and in general, the wave refractive index continues to increase as the waves propagate away from the source [*Draganov et al.*, 1993].

Hypothesis 3 is justified because the propagation of signals with wave normals close to resonance cone implies large values of the wave refractive index, which combined with the rather large (30 km/s) spacecraft velocities, can easily lead to Doppler shifts of the order of $\sim$ 1 kHz. Moreover, the observed monotonic increase or decrease of the Doppler shifted wave frequency away from the source region is consistent with the expected increase in the refractive index as the wave propagates away from the source.

Testing the Hypotheses

A detailed ray tracing analysis is needed to place very tight constraints on the nature of propagation from the source to an observation point. Such an analysis is beyond the scope of this paper and would also require rather precise models of the Neptune's magnetosphere. However, based on geometrical grounds and on the general features of nonducted whistler mode propagation as noted above, it is necessary that the following conditions be satisfied in order for our hypotheses to be true:

1. The signal frequency should be below the local gyrofrequency f_{he} and plasma frequency f_{pe} throughout the region of observation.
2. For obliquely propagating magnetospherically reflected waves to be observable on the spacecraft, the signal frequency (f=3.58 kHz) must be above the local lower hybrid frequency f_{LHR} throughout the region where NBE was observed.

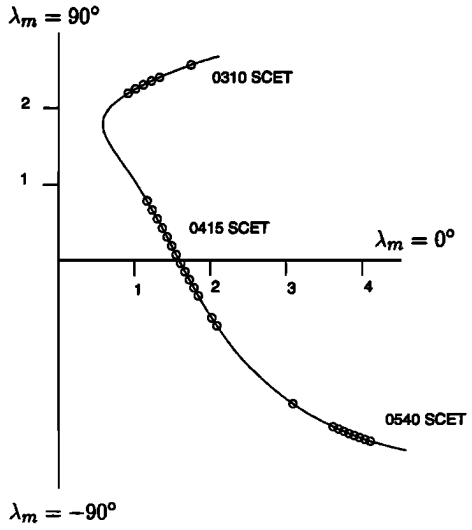

Figure 5. The projection in polar coordinates (R_m, λ_m) of Voyager 2 trajectory in a magnetic meridional plane. R_m is the distance from the origin and λ_m is the angle measured from x axis. The circles indicate locations of Voyager 2 in this plane at times when the 29 wideband frames showing the NBE were obtained.

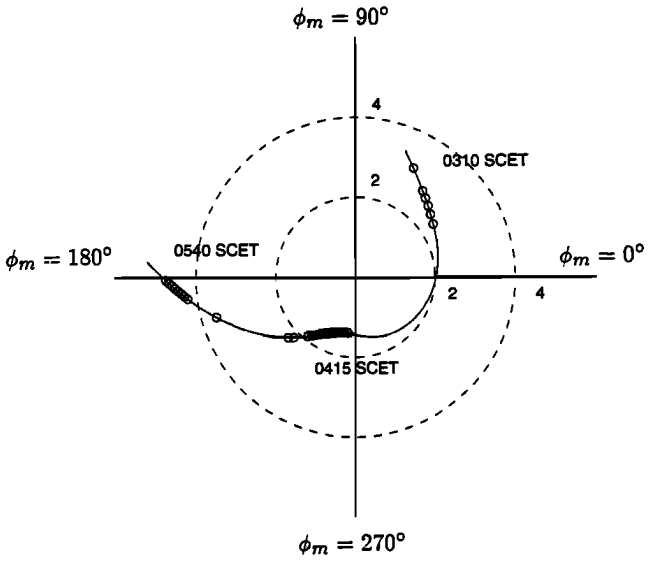

Figure 6. The projection in polar coordinates (R_m, ϕ_m) of Voyager 2 trajectory in the magnetic equatorial plane. The circles indicate locations of Voyager 2 in this plane at times when the 29 wideband frames showing the NBE were obtained.

3. Doppler shifts with correct sign (negative Doppler shifts before 0415 SCET and positive after 0415 SCET) must be possible for waves arriving (from the source region) at the observation point. For times before 0415 (the time when the east-west traversing Voyager 2 crossed the source longitude), the waves would arrive at the observation point with their group ray velocities generally in the W-E direction, and for times after 0415, the waves would arrive at the observation point with their group ray velocities generally in the E-W direction (see Figure 7). Since the wave normal vector and group ray velocity lie in the same plane, this implies that for times before ~0415 SCET, the wave normal vector must possess a component in the W-E direction, and for times after ~0415 SCET wave normal vector must possess a component in the E-W direction. With this restriction on possible wave normal vectors (and taking into account the Voyager 2 velocity vector), it should be possible to obtain observed Doppler shifts.

4. The values of refractive index needed to explain the observations should show a general increase with the increase in the difference between the source and the observation point longitudes.

5. Since waves propagating with wave normal angles close to the resonance cone have large refractive indices, Landau damping of these waves due to their interaction with the thermal plasma population needs to be considered. For the wave parameters needed to explain the observations, Landau damping of nonducted whistler mode waves should be negligible. In our approach we first assume Landau damping to be insignificant and determine the propagation parameters which are consistent with the general features of the nonducted whistler mode propagation and with the observations. Then, using these propagation parameters as the basis of our interpretation, we determine the upper limit on the thermal plasma temperature for Landau damping to be insignificant. Finally, this upper limit on the temperature is compared with that obtained from other independent experiments to test if the initial assumption of insignificant Landau damping is justified. We proceed to demonstrate that all of these conditions are satisfied for our observations for a rather wide range of plasma densities and source locations.

Condition 1: $f < f_{pe}, f_{he}$. Figure 8 shows the local gyrofrequency and the approximate value of the lower hybrid frequency along the Voyager 2 trajectory. Also plotted are the lower and upper cutoff frequencies of the NBE. The figure clearly shows that the local gyrofrequency is above the signal frequency (3.58 kHz) over the entire range, consistent with whistler mode propagation. Absence of NBE in the subsequent wideband frame taken at 0602 SCET, when f_{he} dropped to $\sim$ 2.4 kHz, is also consistent with whistler mode propagation. The absence of signals in wideband frames available before 0310 SCET (the first wideband frame before this time was at 0255 SCET) could be due to spreading losses incurred in propagation from the source to the observation point (note that source and observation points are separated by more than 150° in longitude at this time), or could simply be a temporal effect at the source.

The condition $f < f_{pe}$ requires that $f_{pe,\min} > 3.58$ kHz or $N_{e,\min} > 0.16$ el/cm^3 throughout the observation period ($1.2R_N < r < 5R_N$). This electron density is on the higher side of the typical $N_e \sim 0.001 - 0.1$ measured by the Voyager 2 plasma instrument (PLS) near the closest approach [*Belcher et al.*, 1989], but on the lower side of those suggested by radio and plasma wave observations. For example, radio science instrument indicated electron densities of the order of several hundred cm^{-3} near the closest approach ($R = 1.2R_N$) [*Tyler et al.*, 1989] and the plasma wave instrument indicated electron densities of a few tens to a few hundreds cm^{-3} near closest approach [*Gurnett et al.*, 1990]. The discrepancy between the plasma instrument and these other measurements may be due to the fact that, near the closest approach, the plasma sensor was oriented in such a way so as not to measure the total electron density [*Gurnett et al.*, 1990]. We note that if the average f_{pe} does indeed lie near 3.0 kHz, as suggested by the PLS experiment, then the NBE is not a whistler mode emission and the interpretation presented here is not viable.

Condition 2: $f > f_{LHR}$. An upper limit on the possible electron density can be placed by requirement 2 above that $f > f_{LHR}$ throughout the observation region. The lower hybrid frequency for a two-component plasma is given by

$$f_{LHR} = \left[\frac{m_i}{m_e}\left(\frac{1}{f_{pe}^2} + \frac{1}{f_{he}^2}\right)\right]^{-1/2} \quad (1)$$

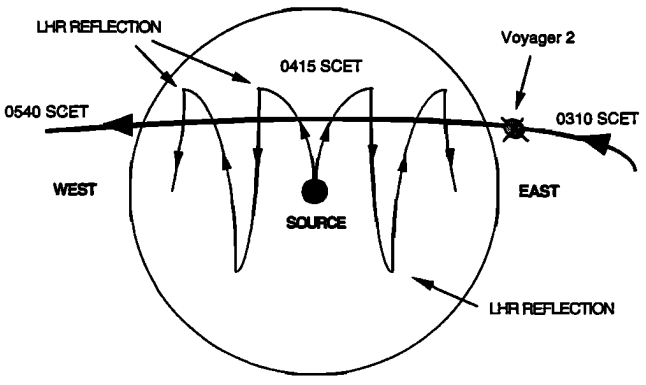

Figure 7. Schematic of multihop nonducted whistler mode propagation (thin lines) of waves from the source region to observation points along the Voyager 2 trajectory (thick line). The source is assumed to be located in a plane near 250° dipole longitude. Voyager 2 crosses this plane around 0415 SCET. Prior to 0415 SCET, waves propagating in the W-E direction would reach Voyager 2 and after this time waves propagating E-W would reach Voyager 2. The waves undergo lower hybrid resonance (LHR) reflections in both the hemispheres when $f = f_{LHR}$, where f_{LHR} is the local lower hybrid resonance frequency.

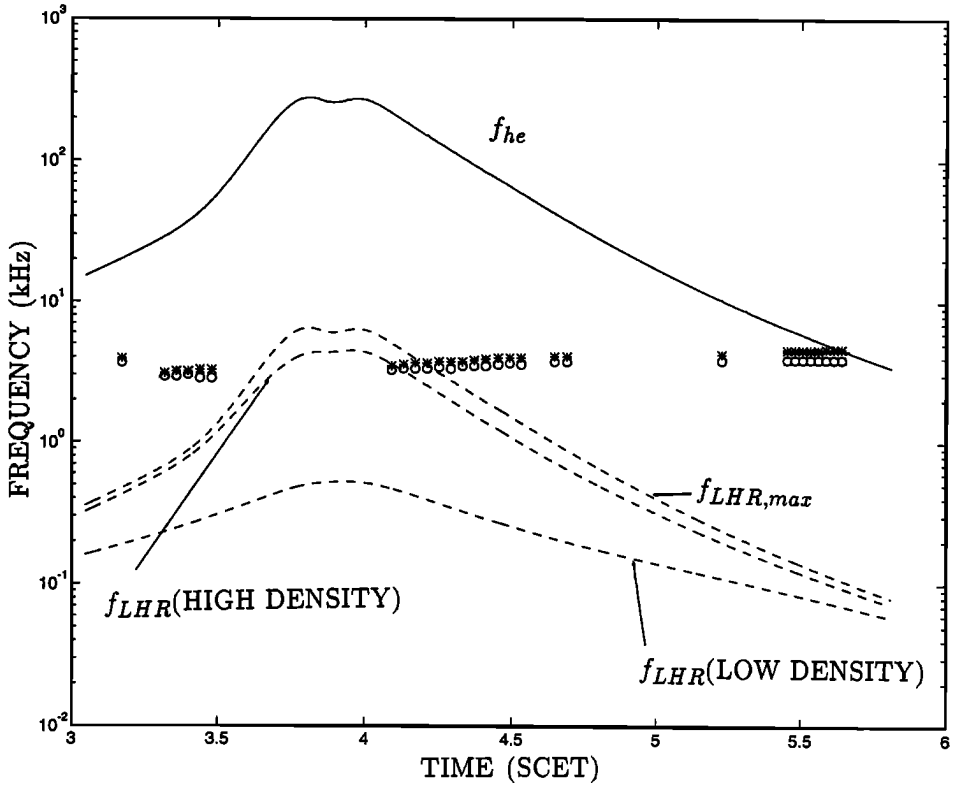

Figure 8. The local gyrofrequency f_{he}, the upper limit on lower hybrid frequency $f_{LHR,\max}$, and the values of f_{LHR} for the low- and high-density models along the Voyager 2 trajectory. Also plotted are the lower (circles) and upper cutoff (asterisks) frequencies of the NBE.

where m_e and m_i are the masses of electron and the assumed ion species. An upper limit on f_{LHR} is obtained when $f_{pe} >> f_{he}$. In this case

$$f_{LHR,\max} = \sqrt{m_e/m_i} f_{he} \tag{2}$$

Assuming H^+ to be the dominant ion, the upper limit on $f_{LHR,\max}$ is plotted in Figure 8 (for heavier ions, $f_{LHR,\max}$ would be smaller than that for H^+). We note that $f_{LHR,\max} > f$ for NBE observed on four wideband data frames collected between 0405 and 0412 SCET. This implies that in order to satisfy condition 2 we must place an upper limit on the possible plasma densities near Voyager 2 locations at these time. Setting f_{LHR} = 3.6 kHz at 0405, and using the measured value of f_{he} at this time we obtain $f_{pe,\max}$= 220 kHz or $N_{e,\max}$=597.5 cm^{-3} at $R = 1.3R_N$. We note that this upper limit is comparable to those indicated by the radio science and the plasma wave instrument at similar radial distances [*Tyler et al.*, 1989; *Gurnett et al.*, 1990].

For our subsequent work it is convenient to adopt a plasma density model, even though our results are not too sensitive to the details of the model. We shall consider two models, low- and high-density models, with a power law dependence:

$$N_e = N_0 \left(\frac{R}{R_N}\right)^{-k} \tag{3}$$

We need densities at two radial distances to determine the constants N_0 and k. For lower radial distances, the low-density model assumes $N_{e,\max}$=1.8 cm^{-3} at $R = 2R_N$ based on the fact that whistlers up to 12 kHz were observed for $R \leq 2R_N$ [*Gurnett et al.*, 1990]. For lower radial distances, the high-density model assumes $N_{e,\max}$=597.5 cm^{-3} at $R = 1.3R_N$ based on our derived upper limit on plasma frequency. For higher radial distances we assume, in both cases, $N_{e,\max}$=0.049 cm^{-3} at $R = 10R_N$ based on the measurement of upper hybrid frequency ($\sim$ 2 kHz) emissions [*Gurnett et al.*, 1989]. This gives us

$$N_0 = 8.47 \text{ cm}^{-3}, \quad k = 2.23, \quad \text{low} - \text{density model} \tag{4}$$

$$N_0 = 2000.00\text{cm}^{-3}, \quad k = 4.61, \quad \text{high} - \text{density model} \tag{5}$$

Figure 8 shows the local lower hybrid resonance frequency for these two models and we note that $f > f_{LHR}$ is satisfied (condition 2).

Condition 3: Doppler shifted signal frequency. We now focus our attention on the problem of obtaining appropriate Doppler shifts for waves that are propagating close to the resonance cone (condition 3). For this purpose it is convenient to define a special reference frame (Figure 9). In this frame the z axis is along the local (measured) magnetic field $\mathbf{B}_0$, the unit vector in the azimuthal direction of the OTD2 model is in the $x - z$ plane and the y axis is determined by the right-hand rule. For a unit vector $\hat{\mathbf{n}}(\theta, \phi)$ in the direction of the wave normal vector, θ represents the wave normal direction with respect to the Neptunian magnetic field and ϕ represents the wave normal direction in the azimuthal direction. For waves propagating close to resonance cone, $\hat{\mathbf{n}}(\theta, \phi) \cong \hat{\mathbf{n}}(\theta_r, \phi)$, where θ_r is the resonance cone angle. When the azimuthal angle ϕ of the wave normal vector lies between $-90°$ and $90°$, it represents a wave propagating in the W-E direction and when the angle ϕ of the wave normal vector lies between $90°$ and $270°$, it represents a wave propagating in the E-W direction. Similarly $0° \leq \phi \leq 180°$ represents waves propagating toward higher L-shells and $180° \leq \phi \leq 360°$ waves propagating toward lower L shells.

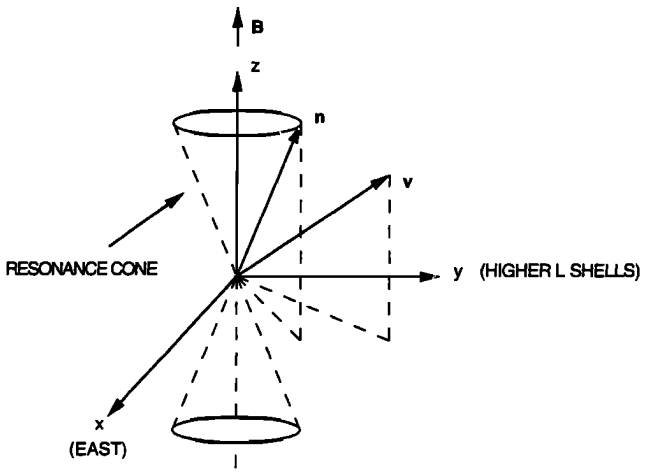

Figure 9. Coordinate frame used to calculate possible wave normal directions. In this frame the z axis is along the local (measured) magnetic field $\mathbf{B}_0$, the unit vector in the azimuthal direction of OTD2 model is in the $x-z$ plane and the y axis is determined by the right-hand rule. The x axis is approximately in the east direction of OTD2 coordinate frame, and the y axis points toward higher L shells.

Since the magnetospherically reflected waves could be moving in either directions (i.e., $\mathbf{B}_0 \cdot \hat{\mathbf{n}} > 0$ or $\mathbf{B}_0 \cdot \hat{\mathbf{n}} < 0$) with respect to the magnetic field, the wave normal direction vector lies on one of the two resonance cones with $\mathbf{B}_0$ or $-\mathbf{B}_0$ as the axis. Thus the observed frequency f_{ob} of a whistler mode signal of frequency f propagating with wave normal vector in the direction of unit vector $\hat{\mathbf{n}}(\theta_r, \phi)$ or $\hat{\mathbf{n}}(180^\circ - \theta_r, \phi)$ is given by

$$f_{ob} = f - \frac{f\mu(\theta_r)V}{c}\hat{\mathbf{n}}(\theta_r, \phi) \cdot \hat{\mathbf{v}}(\theta_v, \phi_v), \tag{6a}$$

or

$$f_{ob} = f - \frac{f\mu(\theta_r)V}{c}\hat{\mathbf{n}}(180^\circ - \theta_r, \phi) \cdot \hat{\mathbf{v}}(\theta_v, \phi_v), \tag{6b}$$

where $\mu(\theta_r)$ is the refractive index, V is the spacecraft speed, and θ_v and ϕ_v are the polar and azimuthal angles of the unit vector parallel to the spacecraft velocity vector. Figure 10 shows plots of V, θ_v and ϕ_v along the Voyager 2 orbit.

The factor $\hat{\mathbf{n}}(\theta_r, \phi) \cdot \hat{\mathbf{v}}(\theta_v, \phi_v)$ determines the sign of the Doppler shift. Since $\hat{\mathbf{n}}$ is constrained to lie on a cone with its axis either parallel or antiparallel to $\mathbf{B}_0$, for given values of θ_r and θ_v, this factor has maximum and minimum values. It can be easily shown that, for wave normal angle $\theta \sim \theta_r$, the factor lies between $\cos(\theta_v - \theta_r)$ and $\cos(\theta_v + \theta_r)$ and for $\theta \sim (180 - \theta_r)$, the factor lies between $-\cos(\theta_v + \theta_r)$ and $-\cos(\theta_v - \theta_r)$. Thus it is clear that both positive and negative Doppler shifts are possible for wave vectors lying close to one or the other of the two possible resonance cones.

It can easily be shown that the expression for the whistler mode resonance cone angle for a two-component cold plasma (electrons and protons and neglecting terms of the order of m_e/m_i) is

$$\tan^2\theta_r = \left(\frac{f_{pe}^2}{f^2} - 1\right) \Big/ \left(1 + \frac{f_{pe}^2}{f_{he}^2 - f^2}\right). \tag{7}$$

An upper limit on the resonance cone is obtained when $f_{pe} >> f_{ce}$. In this case (3) reduces to the more well-known relation

$$\cos\theta_{r,\max} = \frac{f}{f_{he}}, \quad f_{pe} >> f_{he}. \tag{8}$$

When $f_{pe} << f_{he}$, (3) reduces to

$$\tan^2\theta_r = \frac{f_{pe}^2}{f^2} - 1, \quad f_{pe} << f_{he}. \tag{9}$$

Figure 11 shows the variation of θ_r (for f = 3.58 kHz) along the Voyager 2 trajectory for the low- and high-density cases and for the limiting value as given by (8). It is seen from this figure that θ_r is a rather insensitive function of plasma density, leading to the insensitivity of possible wave normal directions to plasma density.

Using the known values of the satellite velocity vector direction (θ_v, ϕ_v), the resonance cone angle θ_r, and the sign of the Doppler shift (i.e., the sign of $f_{ob} - f$), and using (6) we can determine the possible values of azimuthal angle of wave normal vectors that would result in the observed polarity of the Doppler shift for the waves that are propagating in the E-W or W-E direction. Figures 12a and 12b plot the wave normal angles for the low-density case. Figure 12a shows the solution for the case $\mathbf{B}_0 \cdot \hat{\mathbf{n}} > 0$ and 12b shows the solution for the case $\mathbf{B}_0 \cdot \hat{\mathbf{n}} < 0$. Together, these figures show that a solution consistent with condition 3 is possible.

In particular, Figure 12 shows that close to the source in the westward direction solutions are possible for both the cases, whereas further away from the source, solution is possible only for the $\mathbf{B}_0 \cdot \hat{\mathbf{n}} > 0$ case. Close to the source in the eastward direction, solution is possible for the $\mathbf{B}_0 \cdot \hat{\mathbf{n}} > 0$ case, and further away it is possible for $\mathbf{B}_0 \cdot \hat{\mathbf{n}} < 0$. Close to the source, for waves propagating in either direction, the azimuthal directions near -90° and 270° indicate that solutions are possible for waves propagating toward low L shells, whereas away from the source, for waves propagating in either directions, the azimuthal directions near -90° and 270° as well as near 90° indicate that solutions are possible for waves propagating toward both low and high L shells. The very first wideband data frame at 0310 SCET, which shows departure from the monotonic decrease in frequency with time before 0415 SCET, shows that both $B_0 \cdot \hat{\mathbf{n}} > 0$ and $B_0 \cdot \hat{\mathbf{n}} < 0$ cases would be over a wide range of azimuthal angles. The signal observed in this frame was very weak (weakest of the signals observed in all wideband frames) and may possibly be due to scattering of NBE by local plasma inhomogeneities. This could also explain the unusual Doppler shift in this case.

The variation in the emission bandwidth (200-800 Hz) can result from the possible spread in the wave normal direction which

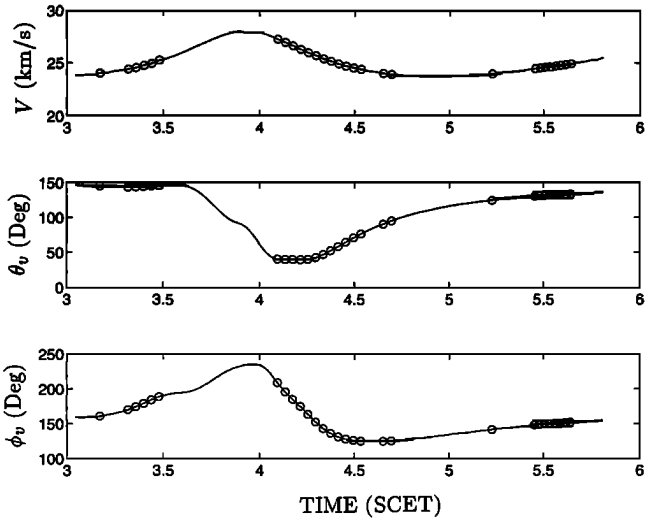

Figure 10. The spacecraft velocity V, and the polar angle θ_v and azimuthal angle ϕ_v (in the coordinate frame shown in Figure 9) of the unit vector $\hat{\mathbf{v}}$ parallel to the spacecraft velocity vector.

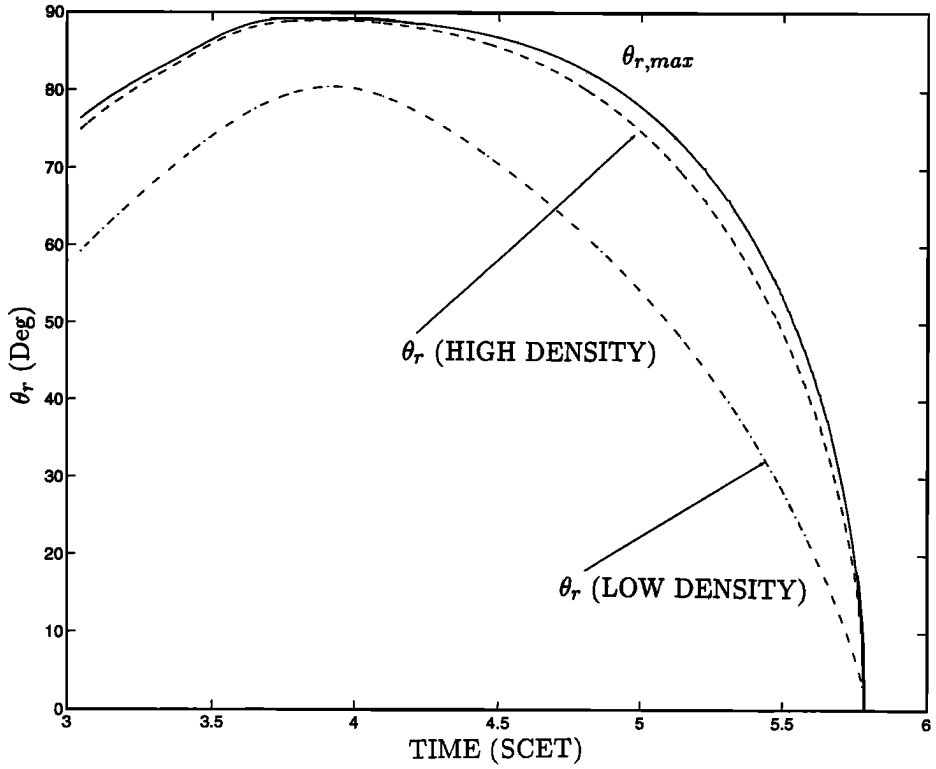

Figure 11. Variation of the resonance cone angle θ_r along the Voyager 2 trajectory for the low- and high-density cases and that for the limiting value of $\theta_{r,\max}$ given by (8).

corresponds to spread in the $\hat{\mathbf{n}} \cdot \hat{\mathbf{v}}$ factor in (6). Rather large bandwidths observed after 0530 SCET are consistent with large spreads in ϕ after 0530 SCET and relatively smaller bandwidths observed at earlier periods are consistent with smaller spreads in ϕ for these periods.

Condition 4: The wave refractive index. To test condition 4, we calculate the minimum refractive index needed to obtain the observed Doppler shift. From (6) we have

$$\mu(\theta_r)_{\min} = \frac{c|f_{0b} - f|}{fV(\hat{\mathbf{n}} \cdot \hat{\mathbf{v}})_{\max}}. \tag{10}$$

Figure 13a plots $\mu(\theta_r)_{min}$ along the satellite trajectory. Consistent with condition 4 we find that the minimum refractive index increase as the Voyager 2 (observation point) moves away from the source. The refractive index value needed to explain the observed Doppler shifts is of the order of a few hundred to a few thousand. Such large refractive indices are commonly observed in the Earth's magnetosphere for whistler mode signals propagating close to the resonance cone [*Bell et al.*, 1994].

Condition 5: The Landau damping. Finally, we consider the question of Landau damping (condition 5). Cold plasma theory predicts an open refractive index surface for $f > f_{LHR}$; thus in principle $\mu \rightarrow \infty$ as $\theta \rightarrow \theta_r$. However, an upper limit on possible values of μ is set by thermal effects. Landau damping of the waves can occur when the parallel phase velocity $\omega/k_{\|} \sim V_{\|}^e$, where $k_{\|}$ and $V_{\|}^e$ are the wave normal vector and thermal electron velocity components along $\mathbf{B}_0$, respectively. This places an upper limit on possible values of μ in terms of electron temperature. We have

$$\mu(\theta_r) \leq \sqrt{\frac{m_e c^2}{k_B T_e}} \sec\theta_r, \tag{11}$$

where m_e and T_e are the electron mass and temperature and k_B and c are the Boltzman constant and velocity of light in vacuum.

As mentioned earlier, we assume that there was no significant Landau damping of the waves and that the upper limit on the thermal plasma temperature can be determined from the requirement for insignificant Landau damping. Equation (11) along with (10) allows us to place an upper limit on the local temperature for insignificant Landau damping.

$$T_{e,\max} \leq \frac{m_e c^2 \sec^2\theta_r}{k_B \mu^2(\theta_r)_{\min}} \tag{12}$$

Figure 13b plots the upper limit on the local temperature as derived from (12). The only available value of T_e is 950° for altitudes below 5000 km obtained from the Voyager 2 radio science experiment [*Tyler et al.*, 1989]. At higher altitudes the temperature could be much lower. At low altitudes ($< 3R_N$) this value (950° K) is much lower than the values of temperature (shown in Figure 13b) above which any significant Landau damping would occur. At higher altitudes the temperature above which any significant Landau damping would occur is about 500°, most probably lower than that expected at higher altitudes at Neptune. Thus our assumption that NBE do not suffer any significant Landau damping appears justified. We note that the observed large dispersion of lightning-generated whistlers at Neptune is also indicative of insignificant Landau damping of whistler mode waves [*Menietti et al.*, 1991].

Results obtained from the high-density model give qualitatively the same results as the low-density case, since the primary difference between the low- and high-density cases is the value of resonance cone angle θ_r in (6), (10), and (12). Since the value of θ_r is not very sensitive to plasma density models, the solutions for wave normal angle are similar in both models. Since the maximum possible refractive index increases with θ_r, higher average electron temper-

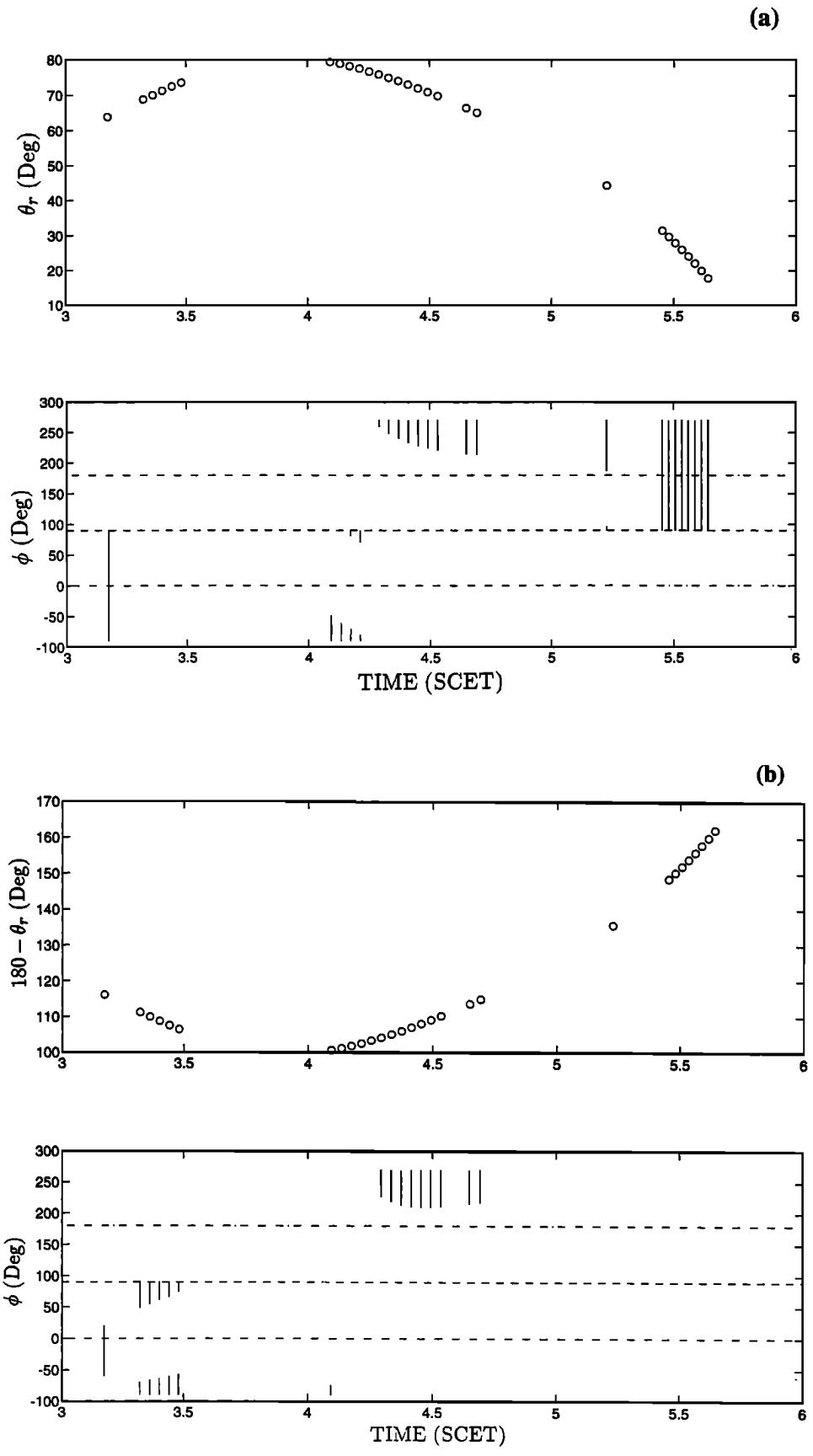

Figure 12. Low-density case: Possible wave normal angles. (a) Solution for the case $\mathbf{B}_0 \cdot \hat{\mathbf{n}} > 0$. (b) Solution for the case $\mathbf{B}_0 \cdot \hat{\mathbf{n}} < 0$. Together, these figures show that a solution consistent with condition 3 is possible.

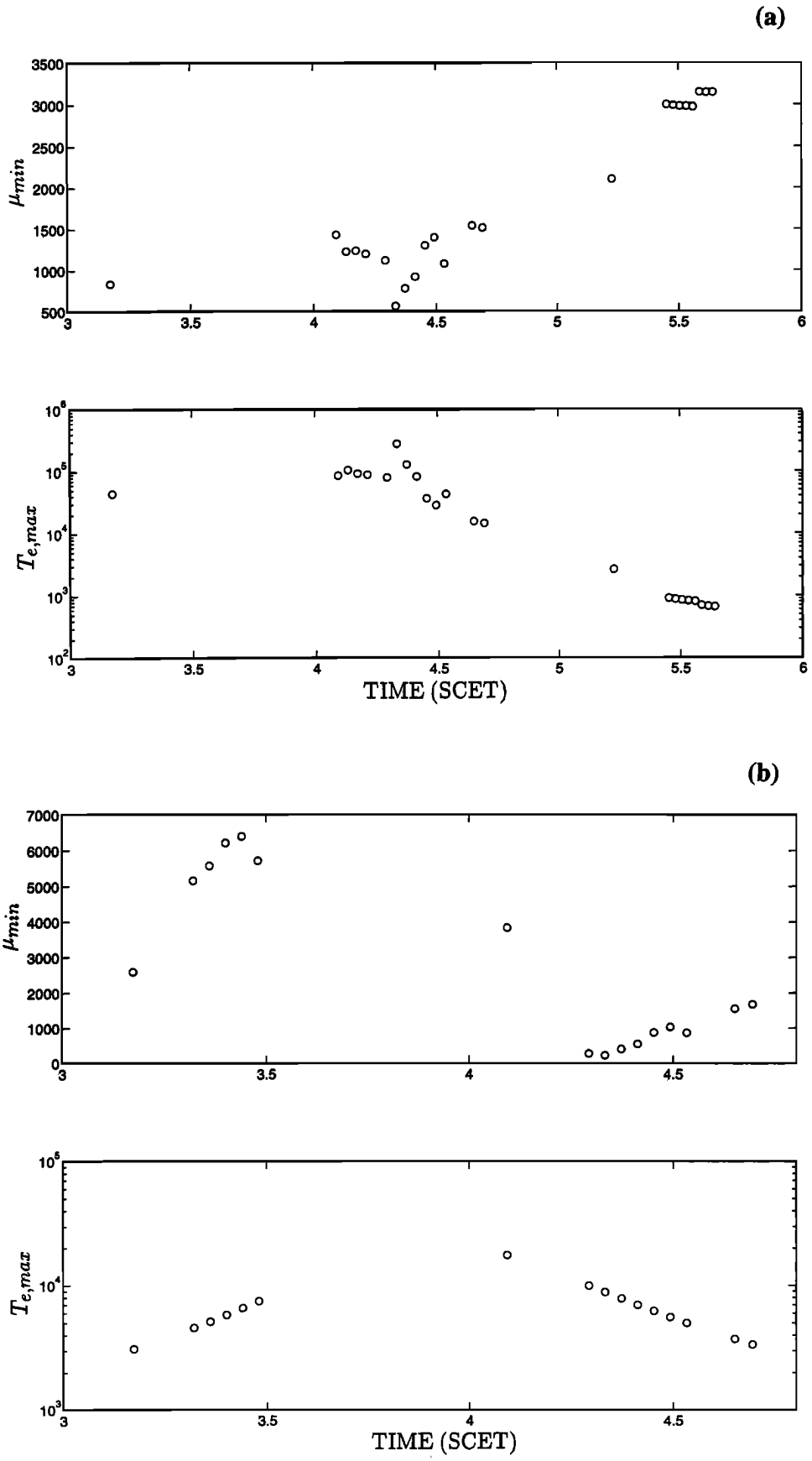

Figure 13. Low-density case: (a) minimum refractive index $\mu(\theta_r)_{\min}$ and the upper limit on the local temperature $T_{e,\max}$ along the Voyager 2 trajectory for the case $\mathbf{B}_0 \cdot \hat{\mathbf{n}} > 0$, and (b) $\mu(\theta_r)_{\min}$ and $T_{e,\max}$ along the Voyager 2 trajectory for the case $\mathbf{B}_0 \cdot \hat{\mathbf{n}} < 0$.

atures are possible before the waves would damp out. Figures 14 and 15 give results for the high-density case. Solutions satisfying conditions 1-5, and similar to those given for the source assumed above, are also possible if the source region is moved to other locations where the strong narrowband emissions were observed (times between 0405 and 0430 SCET).

Based on the results discussed above, we can conclude that the narrowband emissions observed close to Neptune might indeed be whistler mode signals generated somewhere near the dipole longitudes 98°-129°W (246° - 274°W longitude in Neptune coordinate system) corresponding to the longitudes where the strongest signals were observed, and with a source frequency ~3.4-3.8 kHz and source bandwidth ~250-400 Hz. These signals then propagated to other locations in a nonducted whistler mode. The possible L shells of generation region and generation mechanism are discussed in the next section.

Discussion

Multihop propagation, similar to that of NBE described above, of nonducted lightning generated whistlers is commonly observed on satellites in the terrestrial magnetosphere [*Smith and Angerami*, 1968; *Edgar*, 1976]. In the Earth's magnetosphere, *Draganov et al.* [1993] found that rays injected from the ground can propagate about 30° in longitude in 3 hops. *Menietti et al.* [1991] have used a three-dimensional ray tracing program in the Neptunian magnetosphere (using the OTD2 model) to study propagation of lightning energy injected from below the ionosphere. They found in general that the whistlers drift about 10° in magnetic longitude in one hop and cross L shells. In view of these results we might expect that NBE made about $10 - 12$ hops before reaching the distant points near $\sim$ 0300 and $\sim$ 0530 SCET. It is possible that the azimuthal asymmetry of the OTD2 model enables waves to drift long ranges in longitude. Future work on NBE should include three-dimensional ray tracing of multihop whistler mode propagation from a source within the magnetosphere. A convenient formulation of multihop propagation close to resonance cone has recently been given by *Draganov et al.* [1993].

Moses and Coroniti [1991] excluded the possibility of NBE being a whistler mode signal on the grounds that their spectra does not resemble those of naturally occurring whistler mode signals in the Earth's magnetosphere. Commonly observed whistler mode signals of natural origin are lightning-generated whistlers, plasmaspheric hiss, auroral hiss, banded hiss, and chorus. A choruslike emission has also been recently observed both inside and outside the plasmapause on the DE 1 satellite [*Poulsen and Inan*, 1988]. Plasmaspheric hiss [*Thorne et al.* 1973] and auroral hiss [*Gurnett et al.*, 1983] are wideband signals and therefore NBE is probably not similar to these emissions. Whistlers also have a distinctive spectra not similar to that of NBE [*Helliwell*, 1965]. However, NBE spectra are very similar to those of banded hiss or chorus or other emissions [*Poulsen and Inan*, 1988] which are generated in one or more narrow bands [*Burtis*, 1969; *Burtis and Helliwell*, 1975, 1976; *Poulsen and Inan*, 1988]. Figure 16 shows an example of narrowband hiss emission observed on the DE 1 satellite.

The banded hiss and chorus observed by *Burtis* [1969] and *Burtis and Helliwell*, [1975, 1976] were generally found in the low-density region outside the plasmapause for $L \geq 4$ in the early morning to afternoon sector. The frequencies of banded hiss and chorus show a close relationship to the equatorial gyrofrequency along inferred paths of propagation to the points of observation; thus these waves have been assumed to be generated at the equator by a gyroresonance mechanism. In general, the frequency of banded hiss and chorus is 0.1-0.6 f_{heq} where f_{heq} is the equatorial gyrofrequency. The bandwidth of banded hiss and chorus is $10 - 50\%$ of the signal frequency, the median being 16%. Emissions observed by *Poulsen and Inan* [1988] were found for $L \geq 2.4$ both inside and outside the plasmapause in the 0400-0800 local time sector. These emissions share many properties in common with banded chorus, including a close relationship of their frequency to the equatorial gyrofrequency.

It is probable that the NBE are similar to banded chorus or hiss, most likely banded hiss, observed near earth. (If NBE were choruslike, any absence of structure could possibly result from large dispersion due to propagation close to the resonance cone.) We note that some evidence of band structure, often found for banded hiss and chorus, was detected in the narrowband emissions observed close to 0530 SCET (see Figure 1b). If these emissions are indeed similar to banded hiss and chorus, then they might be generated by a gyro-resonance mechanism close to the equator at L shells such that the observed frequency at spacecraft longitudes close to the generation region is $f \sim 0.1 - 0.6 f_{heq}$, where f_{heq} is the Neptunian equatorial gyrofrequency. This allows us to place a limit on the source location in L shell and permits us to determine the resonant particle energies that might have generated these emissions. For a source of frequency 3.58 kHz located in the 111°W dipole meridian, the equatorial gyrofrequency would range from ~36 to 6 kHz. This gives the possible L shell of the source to be $L \sim 2 - 4$ ($R = 1.60 - 3.58 R_N$). Assuming that these emissions are generated at low wave normal angles by the first-order gyroresonance (the same mechanisms that has been proposed for terrestrial banded hiss and chorus), we can estimate the parallel velocity v_{res} of the resonant electrons as follows:

$$v_{res} = c\left(\frac{f_{he} - f}{f\mu}\right), \tag{13}$$

where c is the velocity of light and μ is the whistler mode refractive index for parallel propagation. Refractive index μ depends on N_e, B_0, and wave frequency. Using the measured values of B_0 and computed values of N_e from (4) and (5), we find that for $L = 2$ the parallel resonant electron energies are very high (> 600 keV) and it is unlikely that NBE was generated close to this L shell. For $L = 4$, however, we find that the parallel electron energy is $\sim$ 19 and $\sim$ 2 keV, respectively, for the low-density (0.49 el/cm^3 at $3.58 R_N$) and high density (5.58 el/cm^3 at $3.58 R_N$) cases. Though these values are below the 22-keV threshold of the Voyager 2 Low-Energy Charged Particle (LECP) instrument [*Krimigis et al.*, 1989], there are indications that the electron spectra near 0400 SCET were rather soft and may have peaked below the threshold of the LECP instrument [*Mauk et al.*, 1990].

The results of the analysis of section 3 suggest that NBE might be generated somewhere near $98° - 129°$W dipole longitudes. Assuming that the emission was indeed generated by gyroresonance interactions with energetic electrons near the magnetic equator, and noting that the brightest emission occurred near 0415 SCET when the spacecraft passed close to the equator ($\lambda_m = 12°$), we conclude that 111°W dipole latitude (corresponding to 260°W longitude in the Neptune coordinate system), $\lambda_m = 0$ and $L = 4$ to be the most likely source location, and $f = 3.6$ kHz and 300 Hz to be the likely source frequency and bandwidth, respectively.

The NBE, on the other hand, can lead to pitch angle scattering and subsequent precipitation of energetic electrons via gyroresonance and Landau mechanisms. Close to the source region, where the waves might be generated with small wave normal angles, NBE could scatter and precipitate electrons with parallel energies from a few keV to a few tens of keV via gyroresonance. After one or two magnetospheric reflections, when the wave normal angle and

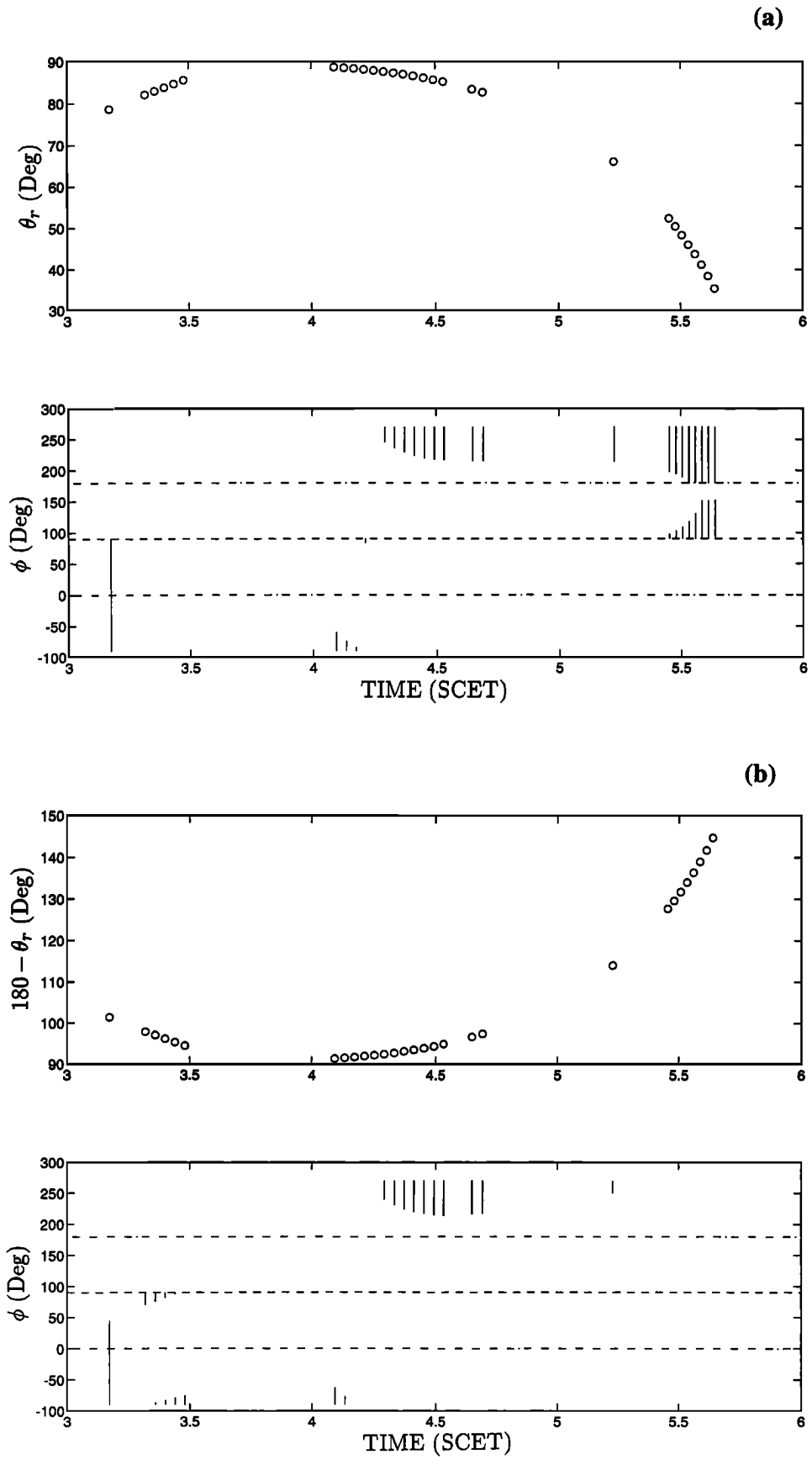

Figure 14. High-density case: Possible wave normal angles. (a) Solution for the case $\mathbf{B}_0 \cdot \hat{\mathbf{n}} > 0$. (b) Solution for the case $\mathbf{B}_0 \cdot \hat{\mathbf{n}} < 0$. Together, these figures shows that a solution consistent with condition 3 is possible.

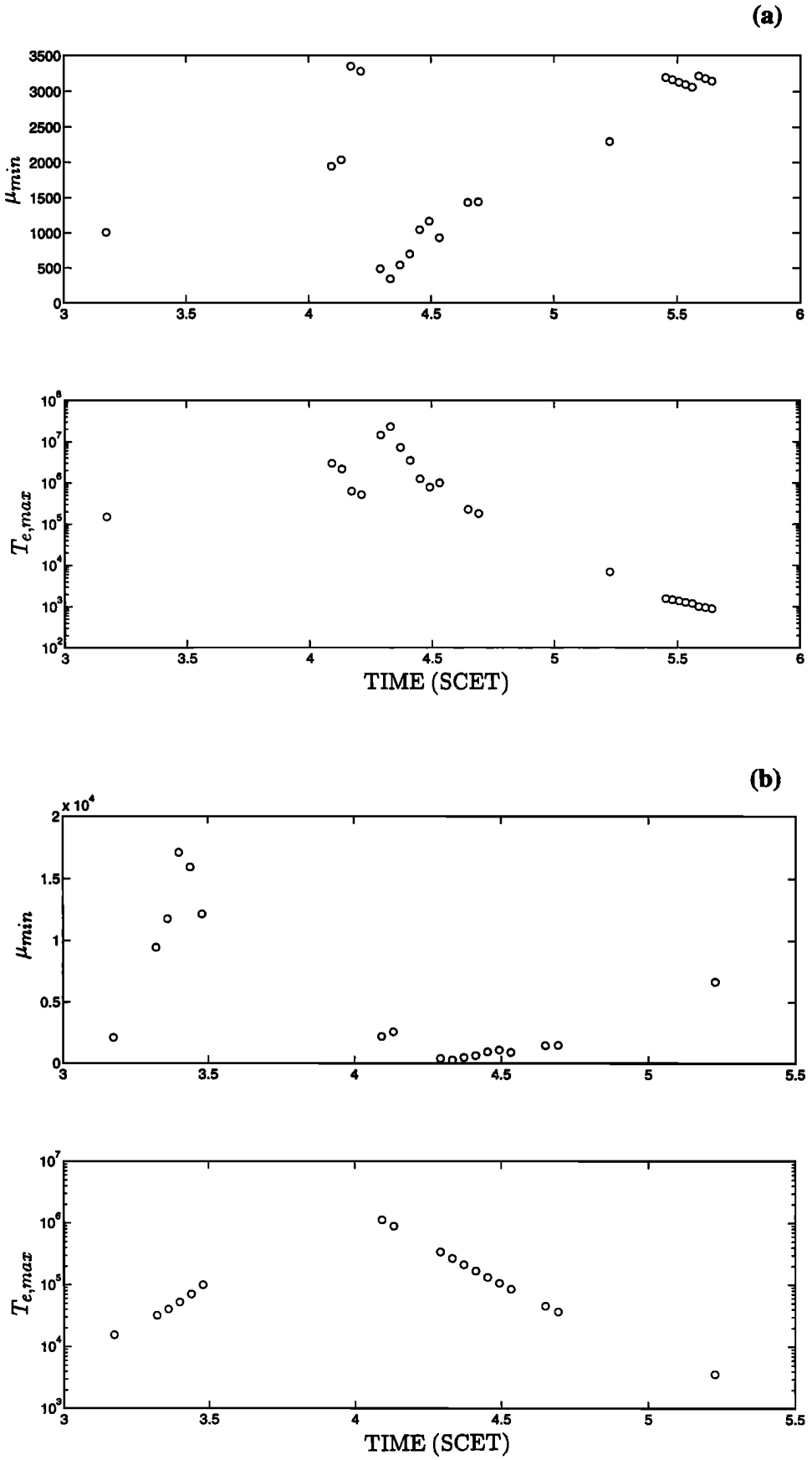

Figure 15. High-density case: (a) minimum refractive index $\mu(\theta_r)_{\min}$ and the upper limit on the local temperature $T_{e,\max}$ along the Voyager 2 trajectory for the case $\mathbf{B}_0 \cdot \hat{\mathbf{n}} > 0$, and (b) $\mu(\theta_r)_{\min}$ and $T_{e,\max}$ along the Voyager 2 trajectory for the case $\mathbf{B}_0 \cdot \hat{\mathbf{n}} < 0$.

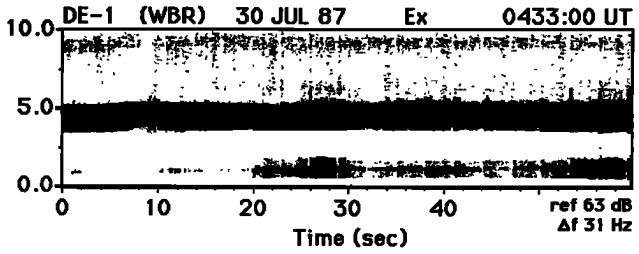

Figure 16. An example of narrowband hiss observed on the DE 1 satellite. DE 1 was located at $L \sim 4$ and $\lambda_m \sim 45°$. The local time was ~0030.

refractive index become large ($\mu > 100$), NBE could scatter and precipitate ~1-100 eV electrons via Landau resonance.

The longitudes (260°W) of our proposed source region are close to the longitude (240°W) of the brighter component of the weak UV aurora observed near Neptune [*Broadfoot et al.*, 1989; *Sandel et al.*, 1990]. This leads to the interesting possibility that the weak UV aurora observed near Neptune could result from the energetic particles precipitated by NBE via wave particle interactions, consistent with the suggestion of *Mauk et al.* [1991] that diffuse precipitation of energetic electrons onto Neptune's atmosphere are the cause of the Neptune's aurora observed near 240°W. Further work, however, is required to test this possibility. In particular, it will be necessary to determine the source L shell (of NBE) and the accessibility of waves to auroral L shells ($L > 8$), and to determine if the amplitude and wave normal direction characteristics of the whistler mode waves reaching the auroral L-shells could precipitate sufficient electron fluxes to cause the observed aurora.

We have provided here a plausible whistler mode interpretation of the NBE. In order to uniquely identify a cold plasma wave mode, it is necessary to have information on local f_{pe}, f_{he}, and the cB/E ratio. In the case of Voyager 2 data from Neptune, we do not have measurement of the wave magnetic component and the measurement of local electron density is highly uncertain. *Gurnett et al.* [1990] have discussed the difficulty of determining the plasma density in the inner magnetosphere of Neptune. At this time the local plasma frequency is believed to lie somewhere between 3 and 150 kHz, a very large range indeed. Thus alternate explanations of NBE, such as those given by *Moses and Coroniti* [1991] can not be ruled out.

In our interpretation we have considered the source of the NBE to be close to the magnetic equator. The spectra of the emission shown in Figures 1b and 2 show a similarity with that of VLF saucer emissions observed at high latitudes in the Earth's magnetosphere [*Moiser and Gurnett*, 1969]. Saucers are also whistler mode emissions propagating near the resonance cone, though the timescales of saucers, typically $\sim 10 - 15$ s, are 2 orders of magnitude shorter than the 2.5 hour duration of the NBE. It is possible that NBE is a saucerlike emission, with a source near the north magnetic pole encountered around 0340 SCET. In this case the drift in frequency is related to the beaming from the source, where progressively higher frequencies are observed at larger distances from the source. Further work is required to test this possibility.

Conclusion and Summary

We have provided a whistler mode interpretation of the narrowband emission observed on Voyager 2 near Neptune. We have shown that the emission could be a whistler mode signal generated by wave-particle interactions in a limited spatial region and propagated to observation points in a nonducted whistler mode. The observed frequency variation of the emission is explained in terms of the Doppler shifts introduced by the motion of the spacecraft. Based on this interpretation, we have determined limits on possible plasma density and temperature for $R < 5R_N$. It is probable that the NBE is similar to narrowband hiss or chorus emissions observed in the terrestrial magnetospheres. Assuming this identification is correct, we have estimated energies of energetic electrons that could generate NBE in the observed frequency range and the energies of electrons that such an emission could precipitate via gyro and Landau interactions. It is possible that the weak UV aurora observed near Neptune could have been caused by the precipitation of energetic particles by the narrowband emission via wave-particle interactions. The lack of precise knowledge of the electron density at Neptune and the unavailability of the wave magnetic field data do not permit a unique identification of the wave mode and thus alternate interpretations of the data can not be ruled out at this time.

Acknowledgments. We gratefully acknowledge D. A. Gurnett and W. S. Kurth for providing the plasma wave data, N. F. Ness for providing the magnetometer data, and M. Kaiser for providing the Voyager 2 orbit and attitude data used in this study. We thank D. L. Carpenter, D. Hinson, R. Simpson and other colleagues in the STAR laboratory for many useful comments and discussions. This work was supported by NASA grant NAGW-2894.

The Editor thanks two referees for their assistance in evaluating this paper.

References

Belcher, J. W., et al., Plasma observations near Neptune: Initial results from Voyager 2, *Science, 246,* 1478, 1989.

Bell, T. F., U. S. Inan, D. S. Lauben, V. S. Sonwalkar, and R. A. Helliwell, DE-1 and COSMOS 1809 observations of lower hybrid waves excited by VLF whistler mode waves, *Geophys. Res. Lett., 21,* 653, 1994.

Broadfoot, A. L., et al., Ultraviolet spectrometer observations of Neptune and Triton, *Science, 246,* 1361, 1989.

Burtis, W. J., Magnetic radiation observed by the OGO-1 and OGO-3 broadband VLF receivers, *Tech. Rep. 3438-1,* Radiosci. Lab., Stanford Univ., Calif., 1969.

Burtis, W. J., and R. A. Helliwell, Magnetospheric chorus: Amplitude and growth rate, *J. Geophys. Res., 80,* 3265, 1975.

Burtis, W. J., and R. A. Helliwell, Magnetospheric chorus: Occurrence pattern and normalized frequency, *Planet. Space Sci., 24,* 1007, 1976.

Cheng, A. F., Global magnetic anomaly and aurora of Neptune, *Geophys. Res. Lett., 17,* 1697, 1990.

Draganov, A. B., U. S. Inan, V. S. Sonwalkar, and T. F. Bell, Whistlers and plasmaspheric hiss: Wave directions and three-dimensional propagation, *J. Geophys. Res., 98,* 11,401, 1993.

Edgar, B. C., The upper and lower frequency cutoffs of magnetospherically reflected whistlers, *J. Geophys. Res., 81,* 205, 1976.

Gurnett, D. A., S. D. Shawhan, and R. R. Shaw, Auroral hiss, Z mode radiation, and auroral kilometric radiation in the polar magnetosphere: DE 1 observations, *J. Geophys. Res., 88,* 329, 1983.

Gurnett, D. A., W. S. Kurth, R. L. Poynter, L. J. Granroth, I. H. Chirns, W. M. Macek, S. L. Moses, F. V. Coroniti, C. F. Kennel, and D. D. Barbosa, First plasma wave observations at Neptune, *Science, 246,* 1494, 1989.

Gurnett, D. A., W. S. Kurth, I. H. Cairns, and L. J. Granroth, Whistlers in Neptune's magnetosphere: Evidence of atmospheric lightning, *J. Geophys. Res., 95,* 20967, 1990.

Helliwell, R. A., *Whistlers and Related Ionospheric Phenomena,* Stanford University Press, Stanford, California, 1965.

Kimura, I., Effects of ions on whistler-mode raytracing, *Radio Sci., 1,* 269, 1966.

Krimigis, S. M., et al., Hot plasma and energetic particles in Neptune's magnetosphere, *Science, 246,* 1483, 1989.

Mauk, B. H., M. Kane, E. P. Keath, A. F. Cheng, S. M. Krimigis, M. H. Acuna, T. P. Armstrong, and N. F. Ness, Energetic charged particle angular distributions near ($r \leq 2R_N$) and over the pole of Neptune, *Geophys. Res. Lett., 17,* 1701, 1990.

Mauk, B. H., E. P. Keath, M. Kane, S. M. Krimigis, A. F. Cheng, T. P. Armstrong, and N. F. Ness, The magnetosphere of Neptune: Hot plasmas and energetic particles, *J. Geophys. Res., 96*, 19061, 1991.

Menietti, J. D., D. Tsintikidis, D. A. Gurnett, and D. B. Curran, Modeling of whistler ray paths in the magnetosphere of Neptune, *J. Geophys. Res., 96*, 19,117, 1991.

Moiser, S. R., and D. A. Gurnett, VLF measurements of the Poytning flux along the geomagnetic field with the Injun 5 satellite, *J. Geophys. Res., 74*, 5675, 1969.

Moses, S. L., and F. V. Coroniti, A mysterious plasma wave emission and the determination of plasma densities in Neptune's inner magnetosphere, *J. Geophys. Res., 96*, 19,013, 1991.

Poulsen, W. L. and U. S. Inan, Satellite observation of a new type of discrete VLF emissions at $L < 4$, *J. Geophys. Res., 93*, 1817, 1988.

Sandel, B. R., F. Herbert, A. J. Dessler, and T. W. Hill, Aurora and airglow on the night side of Neptune, *Geophys. Res. Lett., 17*, 1693, 1990.

Scarf, F. L., and D. A. Gurnett, A plasma wave investigation for the Voyager mission, *Space Sci. Rev., 21*, 289, 1977.

Smith, R. L., and J. J. Angerami, Magnetospheric properties deduced from OGO 1 observations of ducted and non-ducted whistlers, *J. Geophys. Res., 73*, 1, 1968.

Sonwalkar, V. S., *New Signal Analysis Techniques and Their Applications to Space Physics*, Ph.D. thesis, Stanford Univ., 1986.

Sonwalkar, V. S., and U. S. Inan, Lightning as an embryonic source of VLF hiss, *J. Geophys. Res., 94*, 6986, 1989.

Thorne, R. M., E. J. Smith, R. K. Burton, and R. E. Holzer, Plasmaspheric hiss, *J. Geophys. Res., 78*, 1581, 1973.

Tyler, G. L., et al., Voyager radio science observations of Neptune and Triton, *Science, 246*, 1466, 1989.

T. F. Bell, U. S. Inan, and V. S. Sonwalkar, STAR Laboratory, Stanford University, Durand 319, Stanford, CA 94305-4055. (e-mail: bell@nova.stanford.edu; inan@nova.stanford.edu; vss@nova.stanford.edu.)

(Received August 19, 1994; revised October 6, 1994; accepted October 10, 1994.)